\



Propagation dynamics of dipole breathing wave in lossy nonlocal nonlinear media

Jian-Li Guo(郭建丽), Zhen-Jun Yang(杨振军), Xing-Liang Li(李星亮), and Shu-Min Zhang(张书敏)
Citation: Chin. Phys. B, 2022, 31 (**1**): 014203. DOI: 10.1088/1674-1056/ac032c
Journal homepage: http://cpb.iphy.ac.cn; http://iopscience.iop.org/cpb

What follows is a list of articles you may be interested in

Mode splitting and multiple-wavelength managements of surface plasmon polaritons in coupled cavities

Ping-Bo Fu(符平波) and Yue-Gang Chen(陈跃刚)†
Chin. Phys. B, 2022, 31 (**1**): 014216. DOI: 10.1088/1674-1056/ac0e28

Mid-infrared supercontinuum and optical frequency comb generations in a multimode tellurite photonic crystal fiber

Xu Han(韩旭), Ying Han(韩颖), Chao Mei(梅超), Jing-Zhao Guan(管景昭), Yan Wang(王彦), Lin Gong(龚琳), Jin-Hui Yuan(苑金辉), and Chong-Xiu Yu(余重秀)
Chin. Phys. B, 2021, 30 (**9**): 094207. DOI: 10.1088/1674-1056/abf10f

Surface plasmon polaritons induced reduced hacking

Bakhtawar, Muhammad Haneef, and Humayun Khan
Chin. Phys. B, 2021, 30 (**6**): 064215. DOI: 10.1088/1674-1056/abd7e5

Generation of wideband tunable femtosecond laser based on nonlinear propagation of power-scaled mode-locked femtosecond laser pulses in photonic crystal fiber

Zhiguo Lv(吕志国) and Hao Teng(滕浩)
Chin. Phys. B, 2021, 30 (**4**): 044209. DOI: 10.1088/1674-1056/abe231

Design and fabrication of GeAsSeS chalcogenide waveguides with thermal annealing

Limeng Zhang(张李萌), Jinbo Chen(陈锦波), Jierong Gu(顾杰荣), Yixiao Gao(高一骁), Xiang Shen(沈祥), Yimin Chen(陈益敏), and Tiefeng Xu(徐铁峰)
Chin. Phys. B, 2021, 30 (**3**): 034210. DOI: 10.1088/1674-1056/abd757

Propagation dynamics of dipole breathing wave in lossy nonlocal nonlinear media

Jian-Li Guo(郭建丽), Zhen-Jun Yang(杨振军)†, Xing-Liang Li(李星亮), and Shu-Min Zhang(张书敏)

College of Physics, Hebei Key Laboratory of Photophysics Research and Application, Hebei Normal University, Shijiazhuang 050024, *China*

(Received 8 April 2021; accepted manuscript online 20 May 2021)

In the framework of nonlinear wave optics, we report the evolution process of a dipole breathing wave in lossy nonlocal nonlinear media based on the nonlocal nonlinear Schrödinger equation. The analytical expression of the dipole breathing wave in such a nonlinear system is obtained by using the variational method. Taking advantage of the analytical expression, we analyze the influences of various physical parameters on the breathing wave propagation, including the propagation loss and the input power on the beam width, the beam intensity, and the wavefront curvature. Also, the corresponding analytical solutions are obtained. The validity of the analysis results is verified by numerical simulation. This study provides some new insights for investigating beam propagation in lossy nonlinear media.

Keywords: breathing wave, propagation, variational method

PACS: 42.65.Tg, 42.65.Jx **DOI:** 10.1088/1674-1056/ac032c

1. Introduction

Nonlocal optical soliton and breather waves can propagate stably in highly nonlocal nonlinear mediums (HNNMs) when nonlinear self-focusing dynamically balances diffraction, therefore nonlocal nonlinear media have attracted extensive attention recently.[1] A nonlocal medium can exhibit a kind of nonlinear response that the refractive index change of the material at a specific location depends on the intensity of a specific neighborhood at that location.[2,3] In nonlinear media, one kind of the most studied materials are those with high nonlocality, which means that the characteristic length of the nonlinear response is much larger than the beam width, such as nematic liquid crystal mediums (NLCMs),[4,5] nonlinear ion gas,[6] thermal interface,[7] and lead glass.[8] It has a profound influence on the study of propagation dynamics of optical spatial solitons and breathing waves.

The concept of breathing wave plays an important role in explaining and simulating the evolution dynamics of light beams in HNNMs. The theory proposed by Snyder–Mitchell model promotes the intuitive recognition of self-localized wave packets in 1997.[2,9] Previously, the propagation dynamics of beams were well discussed through numerical simulation[10] or inverse scattering modeling and so on.[11] In recent years, people often use Jacobi elliptic function,[12] variable separation method,[13] variational method (VM),[14–16] and other integration algorithms to solve relevant problems. Moreover, some properties of beams in propagation process have been verified in many aspects, such as nonlocalization in dispersion shock wave,[17] Anderson localization,[18] gradient mutation, guide wave distribution coupling, and photon condensation.[19]

Due to foreseeable applications in optical communication, optical switch, and optical tweezers, research of beam propagation characteristics is appealing increasing interests. Studies have shown that nonlocal nonlinearity can support a variety of new soliton states, including bright soliton,[20] surface wave soliton, multimode soliton propagation, helical interaction,[21,22] and so on. The evolutionary characteristics of different types of breathers can be explored and applied. In 2004, Guo *et al.* obtained the evolution of the soliton in an HNNM, focused on the nonlocal nonlinear Schrödinger equation (NNLSE).[9] In 2006, the interaction of nonlocal solitons in NLCMs can be controlled by the degree of nonlocality, which has been proved experimentally by Hu *et al.*[23] In 2011, Ma *et al.* addressed the existence of multipole interface solitons in one-dimensional thermal nonlinear media and found that there exist two kinds of tripole and quadrupole interface solitons and three types of fifth-order interface solitons, respectively.[24] They obtained the analytical solutions of surface solitons and breathers in an HNNM, and obtained the critical power and the period of breathers by numerical simulation.[25] In 2016, Alberucci *et al.* discussed the deviation process of soliton and breather in real materials based on the Snyder–Mitchell model.[26] In 2019, Chen *et al.* predicted the fluctuation of breathers using the VM in an HNNM.[27] In 2020, Shen *et al.* studied dipole solitons and vortex solitons, and discussed the linear anisotropic diffraction in nonlinear media using VM and split-step Fourier transform.[28] The soliton modes and stability of optical pulses in nonlocal nonlinear fused double core planar wave guides have been explored by Gao *et al.*, the Bessel–Gaussian beams modulated by airy mixture have been studied based on vector diffraction theory.[29,30] In our previous works, we discussed the interaction between

†Corresponding author. E-mail: zjyang@vip.163.com

© 2022 Chinese Physical Society and IOP Publishing Ltd

anomalous vortex beams,[31] the evolution of higher-order hyperbolic sine Gaussian solitons and the propagation dynamics of dipole breathers in nonlocal nonlinear media.[32,33] We also theoretically discussed the propagation and interaction characteristics of various moving solitons and soliton arraies, including the breathing state in HNNMs.[34–38]

As a typical representative of HNNMs, NLCMs have received a great deal of attention experimentally and theoretically. For example, the self-trapping of light beams has been tested in NLCMs via the Lagrangian approach.[4] Considering the interaction between solitons and boundary conditions, behavior of accessible solitons with diffusion-like nonlinear response in nonlocal media is investigated.[10] In addition, nonlinear propagation of optical solitons through pure photothermal nonlinearity in a dye doped NLCM has been reported by Kwaśny *et al.*[39] Using the nonlinear response of NLCMs, the molecular direction of optical breather formation and the stability of propagation dynamics are studied by Jung *et al.*[40] The formation, decay and subsequent regeneration of a optical beam in a medium with cubic quintic self interaction and strong dissipative nonlinearity are reported and analyzed by Reyna *et al.*[41] However, the propagation of dipole breathing wave (DBW) in lossy HNNMs has rarely been explored. In this work, we aim to study the evolution dynamics of DBW in a lossy HNNM based on the VM.

The frame of this paper is as follows. In Section 2 we briefly outline the theory and mathematical method on which our investigation are based. In Section 3 the analytical and numerical results of the DBW in lossy highly nonlocal nonlinear systems is carried out. In Section 4 this paper is concluded.

2. Mathematical model

The evolution of optical beams in the HNNM is modeled by the NNLSE[2,34–36,42–44]

$$\mathrm{i}\frac{\partial \Psi}{\partial \tau}+\frac{1}{2}\frac{\partial^2 \Psi}{\partial \xi^2}+\Psi\int_{-\infty}^{+\infty}N(\xi-\xi')|\Psi(\xi',\tau)|^2\mathrm{d}\xi'+\mathrm{i}\frac{\varepsilon}{2}=0, \quad (1)$$

where $\Psi(\xi,\tau)$ is the light field of the paraxial DBW; ξ is transverse coordinate, τ is taken to be the normalized longitudinal propagation distance of the DBW; ε is the loss coefficient of the material. $N(\xi)$ represents the nonlinear response function of the nonlocal media and it satisfies the normalized condition $\int_{-\infty}^{+\infty}N(\xi)\mathrm{d}\xi=1$.[45]

The following transformation is introduced:

$$\Psi(\xi,\tau)=A(\xi,\tau)\exp\left(-\frac{\varepsilon\tau}{2}\right), \quad (2)$$

then Eq. (1) becomes

$$\begin{aligned}&\mathrm{i}\frac{\partial A}{\partial \tau}+\frac{1}{2}\frac{\partial^2 A}{\partial \xi^2}+\exp(-\varepsilon\tau)A\\&\times\int_{-\infty}^{+\infty}N(\xi-\xi')|A(\xi',\tau)|^2\mathrm{d}\xi'=0.\end{aligned} \quad (3)$$

According to the VM, Eq. (3) is an Euler equation

$$J=\int_0^{+\infty}\int_{-\infty}^{+\infty}\mathcal{L}\left(A,A^*,\frac{\partial A}{\partial \xi},\frac{\partial A^*}{\partial \xi},\frac{\partial A}{\partial \tau},\frac{\partial A^*}{\partial \tau}\right)\mathrm{d}\xi\,\mathrm{d}\tau, \quad (4)$$

where $*$ denotes complex conjugation. The variational equation can be written as

$$\delta\int_0^{+\infty}\int_{-\infty}^{+\infty}\mathcal{L}\left(A,A^*,\frac{\partial A}{\partial \xi},\frac{\partial A^*}{\partial \xi},\frac{\partial A}{\partial \tau},\frac{\partial A^*}{\partial \tau}\right)\mathrm{d}\xi\,\mathrm{d}\tau=0, \quad (5)$$

the form of Lagrange function is

$$\begin{aligned}\mathcal{L}=&\frac{\mathrm{i}}{2}\left(A^*\frac{\partial A}{\partial \tau}-A\frac{\partial A^*}{\partial \tau}\right)-\frac{1}{2}\left|\frac{\partial A}{\partial \xi}\right|^2\\&+\frac{1}{2}\exp(-\varepsilon\tau)|A|^2\\&\times\int_{-\infty}^{+\infty}N(\xi-\xi')\left|A(\xi',\tau)\right|^2\mathrm{d}\xi'.\end{aligned} \quad (6)$$

We assume that the initial expression (trial solution) of the DBW in the HNNM takes the form as

$$A(\xi,\tau)=a(\tau)\tau\exp\left[-\frac{\xi^2}{2\omega^2(\tau)}+\mathrm{i}\theta(\tau)+\mathrm{i}c(\tau)\xi^2\right], \quad (7)$$

where $a(\tau)$, $\omega(\tau)$, $c(\tau)$, and $\theta(\tau)$ are the amplitude, beam width, curvature, and additional phase of the DBW, respectively.

Substituting Eq. (7) into Eq. (5), we can acquire the average variational process

$$\delta\int_0^{+\infty}\langle\mathcal{L}\rangle\mathrm{d}\tau=0. \quad (8)$$

The average Lagrangian equation $\langle\mathcal{L}\rangle$ can be written as

$$\langle\mathcal{L}\rangle=\int_{-\infty}^{+\infty}\mathcal{L}\mathrm{d}\tau. \quad (9)$$

In this paper, we adopt the nonlocal response function

$$N(\xi)=\frac{1}{2\omega_\mathrm{m}}\exp\left(-\frac{|\xi|}{\omega_\mathrm{m}}\right) \quad (10)$$

to carry out our investigation. Here, ω_m denotes the characteristic width of $N(\xi)$. This kind response function can be experimentally realized in positive NLCMs.[46–48] It is an extremely hard thing to acquire the accurate propagation expression of the DBW due to the complexity of calculation process. Under the circumstance of strong nonlinearity, Eq. (10) can be rewritten as

$$N(\xi)\simeq\frac{1}{2\omega_\mathrm{m}}\left(1-\frac{|\xi|}{\omega_\mathrm{m}}+\frac{\xi^2}{2\omega_\mathrm{m}^2}\right). \quad (11)$$

Combining Eqs. (9) and (11), after a round of theoretical calculations, $\langle\mathcal{L}\rangle$ can be expressed as

$$\begin{aligned}\langle\mathcal{L}\rangle=&\frac{1}{64\omega_\mathrm{m}^3}\exp(-\tau\varepsilon)a^4(\tau)\omega^6(\tau)\\&\times\left[4\pi\omega_\mathrm{m}^2-7\sqrt{2\pi}\omega_\mathrm{m}\omega(\tau)+6\pi\omega^2(\tau)\right]\end{aligned}$$

$$-\frac{3}{8}\sqrt{\pi}a^2(\tau)\omega(\tau)\left[1+4c^2(\tau)\omega^4(\tau)\right]$$
$$-\frac{1}{4}\sqrt{\pi}a^2(\tau)\omega^3(\tau)\left[3\omega^2(\tau)c'(\tau)+2\theta'(\tau)\right], \quad (12)$$

where the prime shows the first derivative. On the basis of the relevant Euler equation, one obtains

$$2\omega(\tau)a'(\tau)+a(\tau)\omega'(\tau)=0, \quad (13)$$
$$2\omega(\tau)a'(\tau)+a(\tau)\left[5\omega'(\tau)-4c(\tau)\omega(\tau)\right]=0, \quad (14)$$
$$\frac{1}{\omega_{\rm m}^3}\exp(-\tau\varepsilon)a^2(\tau)w^5(\tau)$$
$$\times\left\{4\pi\omega_{\rm m}^2-7\sqrt{2\pi}\omega_{\rm m}^2\omega(\tau)+6\pi\omega^2(\tau)\right\}$$
$$-12\sqrt{\pi}\left[1+4c^2(\tau)\omega^4(\tau)\right]$$
$$+8\sqrt{\pi}\omega^2(\tau)\left[3\omega^2(\tau)c'(\tau)+2\theta'(\tau)\right]=0, \quad (15)$$
$$a^2(\tau)\omega^3(\tau)\left[-24\sqrt{\pi}\omega_{\rm m}^2\omega^2\right.$$
$$\left.+49\sqrt{2}\omega_{\rm m}\omega^3(\tau)-48\sqrt{\pi}\omega^4(\tau)\right]$$
$$+24\exp(\tau\varepsilon)\omega_{\rm m}^3\left[20c^2(\tau)\omega^4(\tau)+10\omega^4(\tau)c'(\tau)\right.$$
$$\left.+4\omega^2(\tau)\theta'(\tau)+1\right]=0. \quad (16)$$

Based on Eqs. (13)–(16), by deformation we can obtain the related equations

$$\frac{\rm d}{{\rm d}\tau}\left[\frac{\sqrt{\pi}}{2}a^2(\tau)\omega^3(\tau)\right]=0, \quad (17)$$
$$\frac{{\rm d}\omega(\tau)}{{\rm d}\tau}=2c(\tau)\omega(\tau), \quad (18)$$

$$\frac{{\rm d}\theta(\tau)}{{\rm d}\tau}=\frac{3}{4\omega^3(\tau)}\left\{\frac{72\pi\omega^3(\tau)}{72\pi\omega^2(\tau)-49\omega_{\rm m}^2}\left[\omega^3(\tau)\omega''(\tau)-3\right]+\left[\frac{56\sqrt{2\pi}\omega_{\rm m}^3}{72\pi\omega^2(\tau)-49\omega_{\rm m}^2}-\frac{84\sqrt{2\pi}\omega_{\rm m}\omega^3(\tau)}{72\pi\omega^2(\tau)-49\omega_{\rm m}^2}\right]\left[\omega^3(\tau)\omega''(\tau)-1\right]\right\}$$
$$+\left\{\frac{\omega_{\rm m}^2\omega(\tau)}{72\pi\omega^2(\tau)-49\omega_{\rm m}^2}\left[245-96\pi+3(32\pi-49)\omega^3(\tau)\omega''(\tau)\right]\right\}, \quad (19)$$
$$\frac{{\rm d}^2\omega(\tau)}{{\rm d}\tau^2}=\frac{\exp(-\tau\varepsilon)}{24\sqrt{\pi}\omega_{\rm m}^3\omega^3(\tau)}\left[24\exp(\tau\varepsilon)\sqrt{\pi}\omega_{\rm m}^3-7\sqrt{2}P_0\omega_{\rm m}\omega^3(\tau)+12\sqrt{\pi}P_0\omega^4(\tau)\right]. \quad (20)$$

According to the definition of the input power $P_0=\int_{-\infty}^{+\infty}|A(\xi,0)|^2{\rm d}\xi$, we obtain the input power without the loss of the DBW

$$P_0=\frac{\sqrt{\pi}}{2}a^2(\tau)\omega^3(\tau), \quad (21)$$

which is a constant based on Eq. (17). $P_\tau=\int_{-\infty}^{+\infty}|\Psi(\xi,\tau)|^2{\rm d}\xi$ is the power during propagation, and it decreases exponentially along propagation distance.

In theory, $a(\tau)$, $\omega(\tau)$, $c(\tau)$, and $\theta(\tau)$ will be acquired because of Eqs. (17)–(20), and the analytical propagation expression of the DBW will be got. In the following section, the propagation expression is solved and the propagation dynamics of the DBW are discussed in detailed. More importantly, the conclusions in this work are apply to else shapes of breathers and can be popularized to other nonlocal optic solitons.

3. Results and discussion

In this section, the effects of the losses on the beam width, light intensity, wavefront curvature, and propagation state will be detailed discussed analytically and numerically.

In Eqs. (17)–(20) we make Eqs. (18) and (20) as zero, i.e., ${\rm d}\omega/{\rm d}\tau={\rm d}^2\omega/{\rm d}\tau^2=0$, the process is the case of no loss of medium. The beam width of the DBW is a constant during propagation, and it is a soliton state. We define the input power as critical power, and it is expressed as

$$P_{\rm c}=\frac{24\sqrt{\pi}\omega_{\rm m}^3}{\omega_0^3\left(7\sqrt{2}\omega_{\rm m}-12\sqrt{\pi}\omega_0\right)}. \quad (22)$$

Here we are dealing with the propagation of a beam in the HNNM, the response degree $\omega_{\rm m}$ of the medium is large, the critical power is relatively accurate.

In the following we discuss the case of loss of the medium, therefore ${\rm d}\omega/{\rm d}\tau\neq0$, the width of the DBW varies during propagation. In Newton's second law, Eq. (20) is used to expresses the motion of a particle with equivalent mass 1.

$$F(\omega)=\frac{1}{\omega^3(\tau)}+\frac{\exp(-\tau\varepsilon)P_0\left[12\sqrt{\pi}\omega(\tau)-7\sqrt{2}\omega_{\rm m}\right]}{24\sqrt{\pi}w_{\rm m}^3}. \quad (23)$$

From Newtonian mechanics, it can be seen that the relationship between the potential $V_{\rm p}$ and the force F in a damped oscillation system is

$$V_{\rm p}(\omega)=-\int F(\omega){\rm d}\omega. \quad (24)$$

We obtain

$$V_{\rm p}(\omega)=\frac{1}{2\omega^2(\tau)}+\frac{7\exp(-\tau\varepsilon)P_0\omega(\tau)}{12\sqrt{2\pi}\omega_{\rm m}^2}$$
$$-\frac{\exp(-\tau\varepsilon)P_0\omega^2(\tau)}{4s_{\rm m}^3}+C. \quad (25)$$

The C is a constant decided by $V_{\rm p}[\omega_0=\omega(0)]=0$ as

$$C=-\frac{\exp(-\tau\varepsilon)}{24\sqrt{\pi}\omega_0^2\omega_{\rm m}^3}\left[-6\sqrt{\pi}P_0\omega_0^4+7\sqrt{2}P_0\omega_0^3\omega_{\rm m}\right.$$
$$\left.+12\exp(\tau\varepsilon)\sqrt{\pi}\omega_{\rm m}^3\right]. \quad (26)$$

With the emergence of nonlinear optics, there are many connections between wave optics and classical mechanics. For

example, the ideas and methods of Lagrange function and Hamiltonian can be used to analyze the optical properties of nonlinear media. In most cases, the experimental results of the mechanical model are consistent with the actual numerical integration results. We give the variation of DBW beam width which is similar to that of classical mechanics, as shown in Fig. 1.

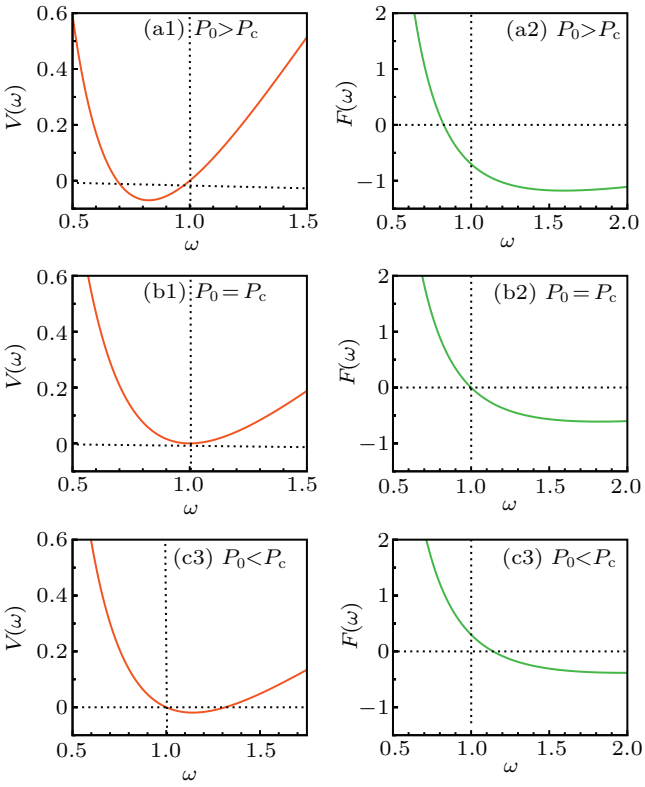


Fig. 1. The equivalent potential energy (column 1) and equivalent force (column 2) varies with beam width under different incident powers. $P_0 = 0.92P_c$ for (a1) and (b1), $P_0 = 1.0P_c$ for (a2) and (b2), $P_0 = 1.08P_c$ for (a3) and (b3). Other parameters are $\omega_m = 10$, $\omega_0 = 1.0$, $\varepsilon = 0.01$, $\tau = 0.1$.

When $P_0 > P_c$, from the perspective of equivalent potential energy, the squeezing effect is stronger than the broadening effect, and the width of the DBW first compresses to a minimum value from the maximum value, and then gradually widens to the maximum value, as shown in Fig. 1(a1). In Fig. 1(a1), the force is less than zero at the input plane, it will be zero when the beam width is compressed to the narrowest, and the process of the beam broadening to the maximum will be relatively slow due to the loss effect, as shown in Fig. 1(a2), where $\omega = 1$ is a root of $V(\omega) = 0$.

When $P_0 = P_c$, the broadening and squeezing of the beam are approximately equal, so the DBW propagates in a soliton-like state, and the equivalent potential energy and equivalent force are also zero at this time, as shown in Figs. 1(b1) and 1(b2). When $P_0 < P_c$, the amplification effect is stronger than the compression effect. The DBW expands from the minimum to the maximum, and then compresses, it is also a periodic process as shown in Fig. 1(c1). The force at the input plane is larger than zero, and the beam width gradually expands to the maximum, as shown in Fig. 1(c2). Although only the relation of the equivalent potential energy and force under a specific loss term is given, it can be verified that this relation is approximately unchanged at other losses and propagation distances. Equal force and potential energy are mainly affected by beam evolution distance and input power, which show different properties. The wave effect of the beam can be controlled for those properties.

The force and potential energy can be regarded as the approximate harmonic motion by graphic analysis. We give the relationship between the equivalent force and potential energy and the propagation distance in Fig. 2 to analyze the relationship more clearly. The power parameters are consistent with Fig. 1, with the increase of propagation distance, the equivalent force becomes smaller and smaller [Fig. 2(a)]. On the contrary, the equivalent potential energy becomes smaller and smaller [Fig. 2(b)]. They are both monotone functions of the propagation distance at the given uniform loss.

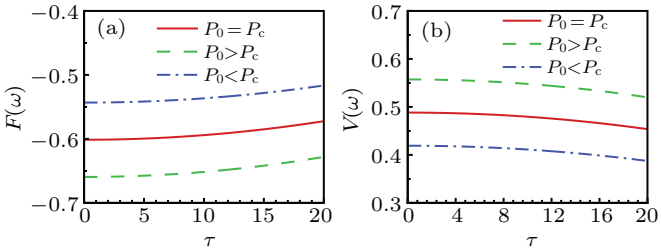


Fig. 2. The equivalent force and equivalent potential energy varies with beam propagation distance under different incident powers. Other parameters are $\omega_m = 10$, $\omega_0 = 1.0$, $\varepsilon = 0.01$.

Generally speaking, the loss factor ε of the HNNM is relatively small, i.e., $\varepsilon \ll 1$, so we consider the approximation $\exp(-\varepsilon\tau) \approx 1 - \varepsilon\tau$. As a result, the influence of the loss on the change of the beam can be considered as perturbation. Hence, we obtain $\omega(\tau) = \omega_1(\tau) + \omega_2(\tau)$, where $\omega_1(\tau)$ is the solution of the beam width when loss is ignored. The beam width of the DBW satisfies a lossless equation in propagation. We can get a width of the DBW, and it can be written as

$$\omega_1(\tau) = \omega_l + (\omega_0 - \omega_l)\cos(\beta\tau), \tag{27}$$

where

$$\begin{aligned}
w_l &= -\frac{1}{2}\left(\frac{B}{2} - \sqrt{\frac{B^2}{4} + t}\right) - \sqrt{\Delta}, \\
B &= \frac{-29w_m}{32\sqrt{2\pi}}, \\
t &= \left(\frac{q}{2} + \sqrt{\frac{q^2}{4} + \frac{p^3}{27}}\right)^{\frac{1}{3}} + \left(\frac{q}{2} - \sqrt{\frac{q^2}{4} + \frac{p^3}{27}}\right)^{\frac{1}{3}}, \\
\Delta &= \left(\frac{B}{2} + \sqrt{\frac{q^2}{4} + \frac{p^3}{27}}\right)^{\frac{1}{3}} + \left(\frac{B}{2} - \sqrt{\frac{q^2}{4} + \frac{p^3}{27}}\right)^{\frac{1}{3}}, \\
p &= -\frac{8w_m^3}{P_0},
\end{aligned}$$

$$q = \frac{49w_{\rm m}^5}{36\pi P_0},$$
$$\beta = \sqrt{\frac{3}{\omega_{\rm l}^4} - \frac{P_0}{2\omega_{\rm m}^3}}.$$

From Eq. (28), one can know that the beam width is a cosine-like function of the propagation length. At the same time, $\omega_2(\tau)$ can be obtained. It is the perturbation caused by loss and satisfies $\omega_2(\tau) \ll 1$ under a certain propagation distance. Thus, we substitute $\omega(\tau) = \omega_1(\tau) + \omega_2(\tau)$ into the equation

$$\omega''(\tau) = \frac{1}{\omega^3(\tau)} + \frac{\omega(\tau)}{2\omega_{\rm m}^3} - \frac{7\sqrt{2}\exp(-\tau\varepsilon)P_0}{24\sqrt{\pi}\omega_{\rm m}^3}. \tag{28}$$

Since $\omega_1(\tau)$ satisfies the relationship given above, for the sake of computing $\omega_2(\tau)$ we take some approximation $1/[\omega_1(\tau) + \omega_2(\tau)]^3 \approx 1/\omega_1^3(\tau) - 3\omega_2(\tau)/\omega_1^4(\tau)$, and $\exp(-\tau\varepsilon) \approx 1 - \tau\varepsilon$, where we ignore the product of $\omega_2(\tau)$ and ε.

When $P_0 = P_{\rm c}$, we assume a relationship like $\omega_1(\tau) = \omega_{1a}$ and $\omega_2(\tau) = \omega_{2a}$, then we obtain $\omega_{1a} = 1$. After calculation, ω_{2a} can be expressed as

$$\omega_{2a} = \frac{\varepsilon\left[\sqrt{K}\tau - \sin(\sqrt{K}\tau)\right]}{K^{3/2}}, \tag{29}$$

where $K = 3 - 12\sqrt{\pi}/(7\sqrt{2}\omega_{\rm m} - 12\sqrt{\pi})$.

When $P_0 \neq P_{\rm c}$, we have a relationship like $\omega_1(\tau) = \omega_{1b}$ and $\omega_2(\tau) = \omega_{2b}$, we obtain $\omega(\tau) = \omega_{1b} + \omega_{2b}$, so ω_{2b} can be acquired as follows:

$$\omega_{2b} = \frac{\tau\varepsilon}{\Lambda}\left(\frac{\omega_{1b}P_0}{2\omega_{\rm m}^3} + \frac{7P_0}{12\sqrt{2\pi}\omega_{\rm m}^3}\right), \tag{30}$$

where $\Lambda = 3/\omega_{1b}^4 - P_0/2\omega_{\rm m}^3$, and ω_{1b} is equal to Eq. (28).

At $P_0 \neq P_{\rm c}$, $\omega(\tau)$ is also divided into two parts, which tells us that considering loss of the media, the beam is oscillatingly widened regardless of the incident power. Thus, the analytical solution of beam width $\omega(\tau)$ in the presence of loss is obtained. In order to demonstrate the validity of our analytical solution of the beam width, the numerical integration of Eq. (2) is carried out, the results are shown in Fig. 3. One sees that the numerical integration based on Eq. (28) and the analytical result is approximate consistency, which shows our variable decomposition and the response function of the correctness of the approximation in Eq. (11).

One can seen that no matter whether the situation is $P_0 > P_{\rm c}$, $P_0 = P_{\rm c}$ or $P_0 < P_{\rm c}$, the beam width tends to widen. The reason is that due to the existence of loss, the power keeps decreasing, which is insufficient to maintain the propagation of soliton or DBW, and the beam width gradually expands. Under different incident powers (as shown in Fig. 3), the DBW is mainly periodically divergent and broadened, which is due to the decrease of the beam amplitude caused by the nonlinearity of the medium. The propagation of the beam is mainly diffracted and broadened, and the fitting two kinds of results is perfect at a certain distance. However, when $P_0 = P_{\rm c}$, the relative error between the numerical and analytical results will increase with the increase of the loss parameter. When $P_0 > P_{\rm c}$, the DBW width expands according to the law of quasi cosine evolution, which compresses first and then expands. When $P_0 < P_{\rm c}$, the beam width evolves in accordance with the quasi-sinusoid relation, and the breather evolves in the form of first broadening and then compression under low power. The propagation distance is greater than 6–7 Rayleigh distances (see Fig. 3). The deviation between the two results begins to increase because of the loss of the medium.

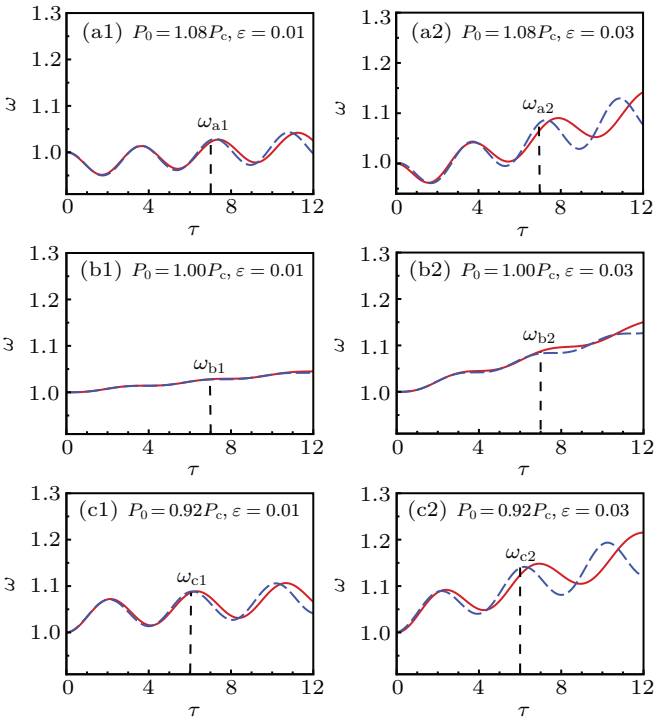


Fig. 3. Evolution of the DBW width $\omega(\tau)$ in the lossy HNNM. Solid line: analytic result; dashed line: numerical integration based on equation initial. Other parameters are $\omega_{\rm m} = 10$, $\omega_0 = 1.0$, $P_0 > P_{\rm c}$ for (a1) and (a2), $P_0 = P_{\rm c}$ for (b1) and (b2), $P_0 < P_{\rm c}$ for (c1) and (c2).

Compared with the analytical results, the deviation between the analytical solution and the numerical solution becomes larger and larger with the increase of the propagation distance of the beam in the lossy medium. At the critical power, the incident DBW exhibits soliton-like propagation. Compared with low power, the analytical and numerical results of high power become better when the loss parameter increases. In order to ensure that the signal is not distorted, we can choose the appropriate distance and incident power to transfer information and energy, so as to avoid errors caused by low power and long distance.

From the above results, we know that the critical power and incident power are different and the beam width is different, the subsequent parameters will also be different. Combining Eqs. (17)–(20) and (28), after some complicated calculations and simplifications, based on the beam width expression

and Euler equation, one can obtain the results of the amplitude $a(\tau)$, the radius of curvature $c(\tau)$, and the additional phase $\theta(\tau)$ of the DBW. When $P_0 = P_c$, we have $a(\tau) = a_1(\tau)$, and light intensity $I(\tau) = I_1(\tau)$:

$$a_1(\tau) = \frac{\sqrt{2}\sqrt{(1+\omega_{2a})^3 P_0 \left[72\pi(1+\omega_{2a})^2 + 49\omega_m^2\right] s^3(\tau)}}{\pi^{1/4}\sqrt{-72\pi(1+\omega_{2a})^8 + 49(1+\omega_{2a})^6\omega_m^2}}, \tag{31}$$

$$I_1(\tau) = \frac{P_0}{\sqrt{\pi}\left\langle 1 + \frac{\varepsilon[-\sin(\tau\sqrt{K})+\tau\sqrt{K}]}{K^{3/2}}\right\rangle}. \tag{32}$$

According to the result of the DBW width, when $P_0 \neq P_c$, we make $a(\tau) = a_2(\tau)$, and $I(\tau) = I_2(\tau)$, the amplitude and light intensity can be received as

$$a_2(\tau) = \frac{\sqrt{2}\sqrt{(\omega_{1b}+\omega_{2b})^3 P_0 \left[72\pi(\omega_{1b}+\omega_{2b})^2 + 49\omega_m^2\right] \omega^3(\tau)}}{\pi^{1/4}\sqrt{-72\pi(\omega_{1b}+\omega_{2b})^8 + 49(\omega_{1b}+\omega_{2b})^6\omega_m^2}}, \tag{33}$$

$$I_2(\tau) = \frac{-\frac{P_0^2}{2\omega_m^3} + \frac{3P_0}{\omega_{1b}^4}}{\sqrt{\pi}\omega_{1b}\left(-\frac{P_0}{2\omega_m^3} + \frac{3}{\omega_{1b}^4}\right) + \tau\varepsilon\left(\frac{7P_0}{12\sqrt{2\pi}\omega_m^3} - \frac{P_0\omega_{1b}}{2\omega_m^3}\right)}. \tag{34}$$

According to the above results, the evolution characteristics of the DBW can be analyzed after the beam intensity is affected by the loss in the propagation process.

In Fig. 4, we give the evolution process of the analytical and numerical results of the DBW intensity with the propagation distance. The corresponding numerical results are also presented in the form of three-dimensional graph in Fig. 5.

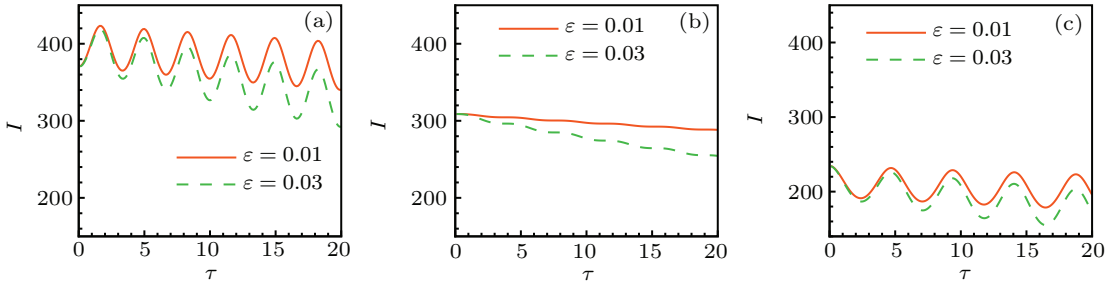


Fig. 4. Evolution of the beam intensity $I(\tau)$ in the lossy HNNM. Solid line: analytical results; dashed line: numerical results. (a) $P_0 = 1.08P_c$, (b) $P_0 = 1.0P_c$, $P_0 = 0.92P_c$. Other parameters are $\omega_m = 10$, $\omega_0 = 1.0$.

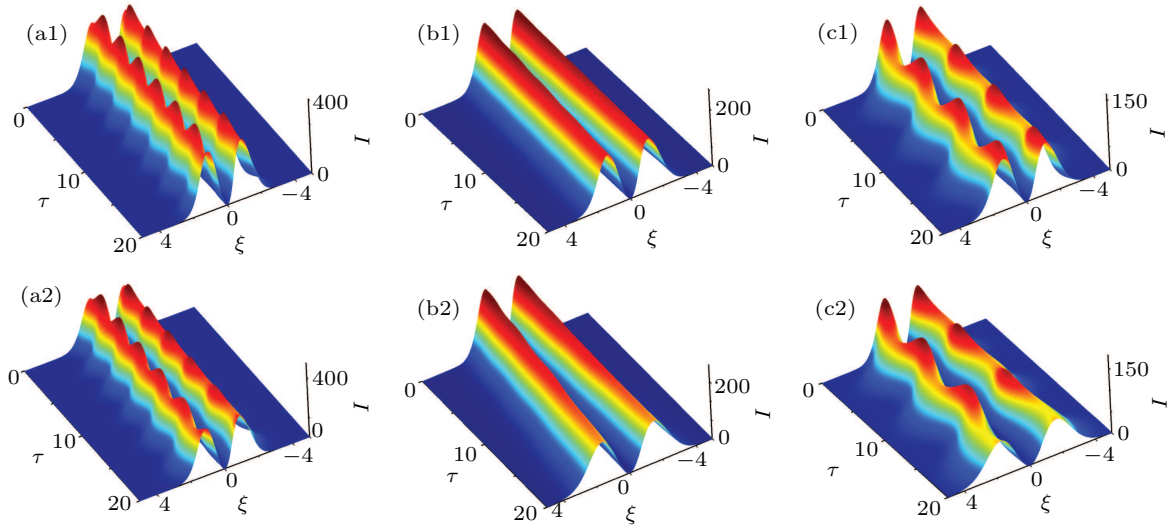


Fig. 5. Numerical integration of the evolution of the beam intensity $I(\tau)$ in the lossy HNNM. Other parameters are $\omega_m = 10$, $\omega_0 = 1.0$.

Due to the existence of the loss, we can know that the DBW width becomes wider with the increase of the propagation distance, at the same time, the central DBW intensity decreases. When the input power is larger than the critical power, the DBW intensity shows the periodic weakening of the sine relation. When the input power is lower than the critical power, it shows the periodic weakening of the cosine relation. The evolution of the light intensity is similar to the periodic weakening of the spring linear harmonic oscillator. When the loss become larger, the central light intensity decreases dramatically, and the influence of the loss on the beam propagation is very obvious.

When $P_0 = P_c$, we have $c(\tau) = c_1(\tau)$, the curvature can be obtained as follows:

$$c_1(\tau) = \frac{\varepsilon[1-\cos(\tau\sqrt{K})]}{2K + 2\varepsilon\left[\tau - \frac{\sin(\tau\sqrt{K})}{\sqrt{K}}\right]}, \tag{35}$$

when $P_0 \neq P_c$, we have $c(\tau) = c_2(\tau)$, so

$$c_2(\tau) = \frac{-MG - \frac{12M\tau\varepsilon Q}{\omega_{1b}^5 G} + \varepsilon Q + \frac{M\tau\varepsilon P_0}{2\omega_m^3}}{2\omega_{1b}G + 2\tau\varepsilon Q}, \tag{36}$$

where

$$\begin{aligned} M &= (\omega_0 - \omega_1)\beta \sin(\tau\beta), \\ Q &= -\frac{\omega_{1b}P_0}{2\omega_m^3} + \frac{7P_0}{12\sqrt{2\pi}\omega_m^2}, \\ G &= \frac{3}{\omega_{1b}^4} - \frac{P_0}{2\omega_m^3}. \end{aligned}$$

Combining the Euler equation and the second derivative of the beam width, we obtain

$$\begin{aligned} \theta'(\tau) &= -\frac{3}{2\omega^2(\tau)} + \frac{\exp(-\tau\varepsilon)P_0}{32\sqrt{\pi}\omega_m^3} \\ &\times \left[16\sqrt{\pi}\omega_m^2 - 21\sqrt{2}\omega_m\omega(\tau) + 12\sqrt{\pi}\omega^2(\tau)\right], \end{aligned} \tag{37}$$

when $P_0 = P_c$, we have $\theta'(\tau)_1 = T_1(\tau)$ and

$$\begin{aligned} T_1(\tau) &= -\frac{3}{2Y^2} + \frac{\exp(-\tau\varepsilon)P_0}{32\sqrt{\pi}\omega_m^3} \\ &\times \left[16\sqrt{\pi}\omega_m^2 - 21\sqrt{2}\omega_m Y + 12\sqrt{\pi}Y^2\right], \end{aligned} \tag{38}$$

where $Y = 1 + 1/K\varepsilon\left[\tau - \sin(\tau\sqrt{K})/\sqrt{K}\right]$, when $P_0 \neq P_c$, we have $\theta'(\tau)_2 = T_2(\tau)$ and

$$\begin{aligned} T_2(\tau) &= -\frac{3}{2D^2} + \frac{\exp(-\tau\varepsilon)P_0}{32\sqrt{\pi}\omega_m^3} \\ &\times \left[16\sqrt{\pi}\omega_m^2 - 21\sqrt{2}\omega_m D + 12\sqrt{\pi}Y^2\right], \end{aligned} \tag{39}$$

the $D = \omega_{1b} + \tau\varepsilon Q/G$.

The evolution process of wavefront curvature is analyzed by comparing the beam width evolution diagram. The contrast between analytical situation and numerical situation for the wavefront curvature is given in Fig. 6. The evolution state of the wavefront curvature is different for the varies powers. In the highly nonlocal environment, when the incident power is closer to the critical power and the loss is small enough (ε less than 0.01), the comparison between the analytical and numerical results is more perfect, see the first column of Figs. 6(a1)–6(c1). The results are no longer accurate within a short distance when the loss is slightly increased, see the second column of Figs. 6(a2)–6(c2). When $P_0 > P_c$, the wavefront curvature evolution obeys the quasi cosine relation, and the radius of DBW curvature first decreases and then increases. When $P_0 < P_c$, the wavefront curvature evolution obeys the quasi sinusoidal relation, and the radius of DBW curvature first increases and then decreases. When $P_0 = P_c$, the radius of DBW curvature is nearly zero, which indicates that the DBW maintains the propagation characteristics similar to soliton.

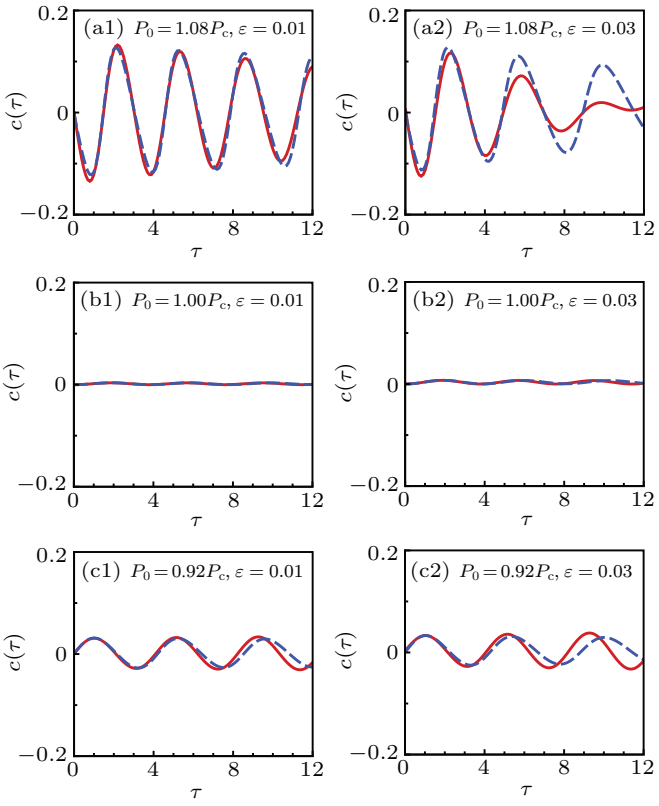


Fig. 6. Evolution diagram of the wavefront curvature $c(\tau)$. Solid line: analytical results. Dashed line: numerical results. (a) $P_0 > P_c$, (b) $P_0 = P_c$, (c) $P_0 < P_c$.

4. Summary

In summary, the propagation expression of the DBW in a lossy HNNM is derived by using the variational method, and the propagation characteristics of the DBW are discussed analytically and numerically. By properly selecting the incident power and the loss coefficient, we analyze the evolution of the beam width, the distribution of the light intensity, and the radius of curvature of the light field. The analytical results are compared with the numerical results, which well reflect the various propagation states of the DBW. In addition, we discuss the influence of loss on the process of information energy transmission. Due to the loss, the beam width of the DBW always expands as it travels farther independent of the input power. The evolution of the beam width is analogous to the relation of particle motion in classical mechanics. The theoretical analysis in this study lays the foundation for the experimental observation of the DBW.

Acknowledgements

This work was supported by the National Natural Science Foundation of China (Grant No. 12074098), the Natural Science Foundation of Hebei Province of China (Grant Nos. A2020205009 and F2020205016), the Science and Technology Project of Hebei Education Department, China (Grant No. ZD2018081), the Chunhui Plan of Ministry of Education of China (Grant No. Z2017020), and the Science Foundation

for Distinguished Young Scholars of Hebei Normal University of China (Grant No. L2017J02).

References

[1] Assanto G 2013 *Nematicons—Spatial Optical Solitons in Nematic Liquid Crystals* (New Jersey: John Wiley Sons)
[2] Snyder A W and Mitchell D J 1997 *Science* **276** 1538
[3] Królikowski W and Bang O 2000 *Phys. Rev. E* **63** 016610
[4] Alberucci A, Kravets N, Piccardi A, Buchnev O, Kaczmarek M and Assanto G 2014 *Opt. Express* **22** 30663
[5] Assanto G, Khan C, Piccardi A and Smyth N F 2019 *Phys. Rev. E* **100** 062702
[6] Misra A P and Shukla P K 2012 *Phys. Rev. E* **85** 1489
[7] Ye F, Kartashov Y V and Torner L 2008 *Phys. Rev. A* **77** 033829
[8] Rotschild C, Cohen O, Manela O, Segev M and Carmon T 2005 *Phys. Rev. Lett.* **95** 213904
[9] Guo Q, Luo B, Yi B, Chi S and Xie Y 2004 *Phys. Rev. E* **69** 016602
[10] Alberucci A, Jisha C P and Assanto G 2014 *Opt. Lett.* **39** 4317
[11] Ablowitz M J and Musslimani Z H 2013 *Phys. Rev. Lett.* **110** 064105
[12] Aslan E C, Tchier F and Inc M 2017 *Superlattice Microst.* **105** 48
[13] Wu H Y and Jiang L H 2019 *Nonlinear Dyn.* **97** 403
[14] Cheng S, Wang Q, Ge L J, Shi J L, Ding H X and Shen M 2011 *Chin. Phys. B* **20** 054206
[15] Chen M N, Zeng S H, Lu D Q, Hu W and Guo Q 2018 *Phys. Rev. E* **98** 022211
[16] Liang G, Cheng W, Dai Z, Jia T, Wang M and Li H 2017 *Opt. Express* **25** 11717
[17] Gentilini S, Ghajeri F, Ghofraniha N, Falco A D and Conti C 2014 *Opt. Express* **22** 1667
[18] Leonetti M, Karbasi S, Mafi A and Conti C 2014 *Phys. Rev. Lett.* **112** 193902
[19] Klaers J, Schmitt J, Vewinger F and Weitz M 2010 *Nature* **468** 545
[20] Alberucci A, Jisha C P, Smyth N F and Assanto G 2015 *Phys. Rev. A* **91** 013841
[21] Gao X H, Wang J, Zhou L, Yang Z J, Ma X, Lu D, Guo Q and Hu W 2014 *Opt. Lett.* **39** 3760
[22] Rotschild C, Segev M, Xu Z, Kartashov Y V, Torner L and Cohen O 2006 *Opt. Lett.* **31** 3312
[23] Hu W, Zhang T, Guo Q, Xuan L and Lan S 2006 *Appl. Phys. Lett.* **89** 071111
[24] Ma X K, Yang Z J, Lu D Q and Hu W 2011 *Phys. Rev. A* **84** 033802
[25] Yang Z, Ma X, Lu D, Zheng Y, Gao X and Hu W 2011 *Opt. Express* **19** 4890
[26] Alberucci A, Jisha C P and Assanto G 2016 *J. Opt.* **18** 125501
[27] Chen M N, Guo Q, Lu D Q and Hu W 2019 *Commun. Nonlinear Sci.* **71** 73
[28] Gao M M and Shen M 2020 *J. Opt.* **22** 025502
[29] Gao Z J and Lin J 2018 *Opt. Commun.* **426** 302
[30] Ding S T and Gao X M 2020 *Appl. Optics* **59** 3673
[31] Yang Z J, Yang Z F, Li J X, Dai Z P, Zhang S M and Li X L 2017 *Results Phys.* **7** 1485
[32] Yang Z J, Dai Z P, Zhang S M and Pang Z G 2015 *Nonlinear Dyn.* **80** 1081
[33] Yang Z J, Zhang S M, Li X L, Pang Z G and Bu H X 2018 *Nonlinear Dyn.* **94** 2563
[34] Yang Z J, Zhang S M, Li X L and Pang Z G 2018 *Appl. Math. Lett.* **82** 64
[35] Yang Z J, Lu D Q, Hu W, Zheng Y Z and Gao X H 2010 *Chin. Phys. B* **19** 124212
[36] Song L, Yang Z, Li X and Zhang S 2018 *Opt. Express* **26** 19182
[37] Song L, Yang Z, Zhang S and Li X 2019 *Opt. Express* **27** 26331
[38] Song L, Yang Z, Zhang S and Li X 2019 *Phys. Rev. A* **99** 063817
[39] Kwasny M, Karpierz M A, Assanto G and LaudynKwasny U 2020 *Opt. Lett.* **45** 2451
[40] PS Jung P S, Izdebskaya Y V, Shvedov V G, Christodoulides D N and Krolikowski W 2021 *Opt. Lett.* **46** 62
[41] Reyna A S, Baltar H, Bergmann E, Amaral A M and Araújo C B D 2020 *Phys. Rev. A* **102** 033523
[42] Nikolov N I, Neshev D, Bang O and Krolikowski W Z 2003 *Phys. Rev. E* **68** 036614
[43] Zeng S, Chen M, Zhang T, Hu W, Guo Q and Lu D 2018 *Phys. Rev. A* **97** 013817
[44] Dai Z, Yang Z, Ling X, Zhang S, Pang Z, Li X and Wang Y 2017 *Sci. Rep.* **7** 122
[45] Guo Q, Luo B, Yi F, Chi S and Xie Y 2004 *Phys. Rev. E* **69** 016602
[46] Xu Z Y, Kartashov Y V and Torner L 2005 *Opt. Lett.* **30** 3171
[47] Skupin S, Bang O, Edmundson D and Krolikowski W 2006 *Phys. Rev. E* **73** 066603
[48] Zhong L H, Li Y Q, Chen Y, Hong W, Hu W and Guo Q 2017 *Sci. Rep.* **7** 41438